A Bi-Level Capacity Optimization of an Isolated Microgrid With Load Demand Management Considering Load and Renewable Generation Uncertainties

GUOLONG MA[ID], **ZEXIANG CAI**[ID], **PENG XIE**[ID], **PING LIU**[ID], **(Student Member, IEEE)**,
SIYANG XIANG, YUYAN SUN, CAISHAN GUO[ID], **(Student Member, IEEE), AND GUANQUAN DAI**

School of Electric Power, South China University of Technology, Guangzhou 510640, China

Corresponding author: Zexiang Cai (epzxcai@scut.edu.cn)

ABSTRACT Aiming at capacity optimization of an isolated microgrid, this paper establishes a bi-level capacity optimization model that considers load demand management (LDM) while comprehensively considering load and renewable generation uncertainties. The uncertainties in this paper are brought by the source and load on the same timescale, as well as by the different characteristics of uncertainty presented over different timescales. For long timescales, the problem of source/load random uncertainty is solved using the stochastic network calculus theory to meet the energy balance constraints. For short timescales, we primarily aim to resolve the problem of power balance at the operation level, considering the uncertainty of source/load prediction errors and the impact of LDM. Particularly, by controlling the interruptible and shiftable loads, the LDM can optimize load characteristics, reduce operation costs, and increase system stability. The bi-level optimization model established in this paper is analyzed with regard to energy and power balance constraints, and the proposed mixed integer linear programming (MILP) model is solved by utilizing the CPLEX solver to minimize the investment cost. A typical microgrid, comprising a wind turbine (WT), a photovoltaic panel (PV), a controllable micro generator (CMG), and an energy storage system (ESS), is taken as an example to study capacity optimization problems. The simulation results verify the rationality and effectiveness of the proposed model and method.

INDEX TERMS Capacity planning, isolated microgrid, load demand management, uncertainties.

NOMENCLATURE

$t, \Delta t, T$	Index, duration and number of time intervals, respectively ($T = 24$ h and $\Delta t = 1$ h).
$C_{\text{operation}}, C_{\text{investment}}$	Operation and Investment cost of the microgrid.
C_{DRE}, C_{ESS}, C_F	Investment cost of DRE, ESS and CMG, respectively.
C_R, C_f, C_{DR}	Operation cost of ESS CMG and LDM, respectively.
$C_{A\&O}$	Total cost of investment and operation of the microgrid.
$\eta_{pv}, \eta_{wind}, \eta_f$	Unit capacity cost of the PV, WT, and CMG, respectively
η_B, η_P	Cost of unit energy capacity and unit power capacity of ESS.
η_{inv}	Inverter cost coefficient.
η_D	Equivalent daily coefficient.
d	Discount rate.
s, S	Index and set of stochastic scenes.
$P_{\text{PV\_unit}}, P_{\text{WT\_unit}}, P_{\text{F\_unit}}$	Power rating of PV, WT and CMG unit, respectively.
B_{ESS}, P_{ESS}	Energy and power ratings of ESS unit.
$N_{\text{PV}}, N_{\text{WT}}, N_F, N_{ESS}$	The number of typical units such as PV, WT, CMG and ESS.
a, b, c	Price coefficients of CMG.

$P_{s,L,t}, P_{s,DER,t}$	Load demand and DER output at time t in the s_{th} scenario, respectively.
$P_{s,i,t}$	Power output of CMG at time t in the s_{th} scenario.
$P_{s,ESS,t}$	Charging/discharging power of ESS at time t in the s_{th} scenario.
$B_{s,ESS}$	Total energy of ESS in the s_{th} scenario.
$SOC_{s,ESS,t}$	State-of-charge (SOC) of ESS at time t in the s_{th} scenario.
$\underline{SOC_{s,ESS}}, \overline{SOC_{s,ESS}}$	Upper and lower SOC limits of ESS in the s_{th} scenario.
η_c, η_d	Charging and discharging efficiency of ESS.
$SOC_{s,ESS,0}$	Initial ESS SOC on each day in the s_{th} scenario.
$\underline{P_{s,i}}, \overline{P_{s,i}}$	Upper and lower power limits of CMG in the s_{th} scenario.
$\underline{P_{s,DER}}, \overline{P_{s,DER}}$	Upper and lower power limits of DER in the s_{th} scenario.
$\underline{P_{s,ESS}}, \overline{P_{s,ESS}}$	Upper and lower power limits of ESS in the s_{th} scenario.
$\varepsilon_s^u(x), \varepsilon_s^l(x)$	Boundary function of the upper and lower limits of the uncertainty power output, respectively.
$\varepsilon_d^u(x), \varepsilon_d^l(x)$	Boundary function of the random upper and lower bound curves of the power demand, respectively.
$\varepsilon_{s\_combined}^u$	Boundary function of the upper limits of the uncertainty combined power output.
$\varepsilon_{d\_combined}^l$	Boundary function of the random lower bound curves of the combined power demand.
$\beta_{combined}^u(s)$	The upper bounds of the cumulative output of combined uncertainty sources during the statistical period $[0,s]$.
$\alpha_{combined}^l(s)$	The lower bounds of the cumulative combined load demand during the statistical period $[0,s]$.
$S(t), D(t)$	The cumulative power of the uncertainty power supply and load demand in the period $[0,t]$, respectively.
$\alpha * (t)$	The horizon LOEP index.
sup	Supremum operation.
H_i	A shiftable time window during a day.
H_n	An ordinary operation period of the shiftable device.
H_m	A fixed time window load that is not participating in shifting scheduling.

N_j	Number of the j_{th} type of the shiftable devices.
P_j	The active power of the j_{th} type of the shiftable devices.
D_j	Length of use of the j_{th} type of the shiftable devices.
G_j	The j_{th} type of the shiftable devices needs to continue using power at the initial time of scheduling.
W_j	Energy consumption required for the shiftable load.
H_{IL}	The set of interruptible time periods.
$U(t)$	Whether the contract management response is executed at the sampling point t.
P_{NLC}	Uncontrollable load power.
$\overline{R_{Ab}}$	Upper ratio of power curtailment of WT and PV.
$E_{G,T,s\in S}$	Total power generation of the DER during scheduling period T.
$E_{load,T,s\in S}$	Total load demand during the dispatch period T (not considering LDM).
$E_{F,T,s\in S}$	Total power generation of the CMG within the scheduled time period T.
$E_{IL,T,s\in S}$	Total interrupted power of the interruptible load during the dispatch period T under LDM conditions.
$E_{C,T}$	Actual consumption of renewable energy.
$E_{AWAV,T}$	Total amount of the curtailed energy.
$r_{k,t}$	Coordination factor
N_k	Uncertainty degree of the simulation scenario for the uncertain source k.

I. INTRODUCTION

A microgrid is a small-scale power distribution system composed of distributed energy, energy conversion devices, loads, and monitoring and protection devices, which can generally operate in grid-connected mode or in island mode. Specially, an isolated microgrid, which is composed of photovoltaic (PV)/wind turbines (WT), energy storage, and diesel units, can solve power supply problems for remote areas without electricity; therefore, more countries and regions are developing this type of microgrid project. For an isolated microgrid, reasonable planning for different types of distributed generators and capacity allocation of energy storage systems (ESSs) helps to reduce the operating costs of the microgrid and improve the energy efficiency [1]–[3].

The distributed renewable energy (DRE) output and load demand are both random and uncertain; thus, the load and renewable generation uncertainty problems in the isolated microgrid capacity planning process primarily arises from the following two sources: 1) multiple uncertain sources, i.e., the DRE output and load demand, and 2) the distinguishing characteristics of uncertainty occurring on different timescales. In addition, the microgrid must consider the impact of the

operation strategy at the planning stage, but during the operation process, the microgrid must be constrained by the system configuration scheme. Thus, the planning design and operation optimization problems are highly coupled, resulting in multiscale uncertainty coupling (MSUC) in microgrid planning. Additionally, with the advancement of marketization processes, a series of load-side control measures, such as load demand management (LDM) and demand response (DR), are incorporated into the operation control of power grids, which have become indispensable approaches for achieving an energy and power balance between supply and demand [4]–[10].

Microgrid planning is an important issue for microgrids. This planning generally aims to minimize planning costs [11] or environmental emissions [12]; or to maximize profit and reliability [13]. In microgrid planning, one must determine the capacity and location of the optimal distributed generation resources [14], the ESS size [15], [16], the transmission power at the connection point with the utility grid, etc.

Currently, relevant research on the capacity planning of microgrids has resulted in useful explorations. To address source and load uncertainty, a stochastic model is proposed by considering the randomness of renewable energy and the uncertainty of load forecasting, achieving optimal capacity planning for distributed generators and energy storage devices in a residential microgrid via mixed integer linear programming (MILP) with the minimum planning cost in [17]. In [18], Monte Carlo simulations are used to simulate the random uncertainties of wind speed, electricity cost and load, and a particle swarm optimization algorithm is applied to realize an optimal capacity allocation for a distributed generation system and battery in a smart home. In [19], an iterative search is performed with maximum reliability and minimum investment cost as the objectives, obtaining the optimal capacities of distributed generators and energy storage. Reference [20] introduces the approach of using two-stage stochastic programming to incorporate the various possible scenarios for renewable energy generation and cost in the planning of microgrids to tackle the uncertainty in planning and designing renewable energy-based microgrids. In [21], an optimal operation planning method taking into consideration the uncertainties of renewable power generation and load demand is proposed and studied. For load management, user-side power consumption behaviors can also be regulated by the DR, such that the load characteristics are matched to the power generation characteristics, including those of WTs and PVs, thereby reducing the capacity allocation of the microgrid [7]–[10]. Reference [22] presents a bi-level model for a distribution network and renewable energy expansion planning under a DR framework. Reference [23] presents a time-shifting desalination load in an islanded microgrid to track renewable energy generation; it was demonstrated that the consideration of a time-shifting desalination load can reduce redundant investments to maximize resource utilization. In [24], a trilevel expansion planning framework is presented for an islanded microgrid; this framework includes demand expansion, capacity optimization and operation optimization. In addition, reference [25] considers the flexibility of the DR to meet users' comfort and applies a genetic algorithm (GA) and MILP simultaneously to solve two-stage optimization regarding utilities' profits and customers' satisfaction. However, these studies do not consider the different characteristics of uncertainties presented by different sources and different timescales; Furthermore, LDM affects the operational characteristics of different types of power supplies at the operational level, which in turn affects the long-term capacity planning results of the system.

In particular, to overcome the abovementioned shortcomings, an isolated microgrid bi-level capacity optimization model is established in this paper to comprehensively consider the influence of MSUC. For long timescales, the problem of energy balance in the planning process is solved using the stochastic network calculus theory for source/load random uncertainty problems. For short timescales, this paper primarily aims to solve the problem of power balance during operation. Specifically, for the stochastic uncertainty characteristics of source and load presentation for the long-timescale capacity planning problem, the stochastic network calculus theory is used to ensure energy balance in an isolated microgrid. For the short-timescale power balance problem, the prediction error uncertainty and the impact of LDM are considered. The prediction error uncertainty is characterized by multiple source and load scenarios via Monte Carlo simulations. Particularly, LDM can optimize the load characteristics by controlling interruptible and shiftable loads, reducing operation costs and increasing system stability. A typical microgrid includes a WT, a photovoltaic panel (PV), a controllable micro generator (CMG) and an energy storage system (ESS). Specially, the microgrid model in this paper is used to study the capacity optimization problem to verify the rationality and effectiveness of the proposed model and method.

The main contributions of this paper are summarized below.

- We comprehensively consider load and renewable generation uncertainties, which are characteristics called MSUC in our model. The influence of MSUC is determined by considering the uncertainties brought by the source and load on the same timescale, as well as the different characteristics of uncertainty presented over different timescales.
- We utilize the business flow arrival process and departure process in the network calculus theory to mimic the uncertain power supply and load demand and then solve the problem of energy balance under the influence of the source/load stochastic uncertainty in the microgrid planning process using the network calculus theory.
- At the operation level, we develop controllable load models including an interruptible load and a shiftable load, and investigate the impact of LDM on the capacity planning for an isolated microgrid.

- A bi-level optimization model that fully considers MSUC and LDM is established, with the goal of achieving an environmentally friendly and cost-effective isolated microgrid.

The rest of this paper is organized as follows. Differential characterization models that reflect the different characteristics of MSUC are presented in Section II. Section III presents a mathematical characterization of the load model under the influence of LDM. A bi-level capacity optimization model for an isolated microgrid that considers LDM and MSUC is established in Section IV. Section V gives the solution method to the proposed model, followed by the model linearization. Numerical simulations and data analyses are reported in Section VI. Finally, Section VII concludes the paper.

II. DIFFERENTIAL CHARACTERIZATION OF MULTISCALE UNCERTAINTY COUPLING

A. LONG-TIMESCALE SOURCE-LOAD RANDOM UNCERTAINTY MODEL

For the problem of source-load random uncertainty, this paper mainly considers meteorological data information such as ambient temperature, daily radiation intensity and wind speed in the planned area. The power output from sources of uncertainty (mainly wind power, photovoltaic) is calculated by the method stated in [26], [27]. In addition, this paper considers the uncertainty power supply and load demand in the isolated microgrid system as the abstraction of the network calculus theory business flow arrival process and departure process, respectively [28]. Therefore, the function $S(t)$ is defined to describe the cumulative power of the uncertainty power supply in the period $[0, t]$. The function $D(t)$ is defined to describe the cumulative demand of the load during the period $[0, t]$. Obviously, $S(t)$ and $D(t)$ are non-decreasing functions, and $S(0) = D(0) = 0$. Further, the functions $\beta_w^u(t)$ and $\beta_w^l(t)$ are respectively used to describe the upper and lower bounds of the cumulative output of a single wind turbine during the statistical period; the functions $\beta_p^u(t)$ and $\beta_p^l(t)$ are respectively used to describe the upper and lower bounds of the cumulative output of a single PV during the statistical period; and the functions $\alpha^u(t)$ and $\alpha^l(t)$ are respectively used to describe the upper and lower bounds of the cumulative demand of the load during the statistical period. The specific characterization of the upper and lower bounds of the cumulative energy is shown in Fig. 1. We can obtain the upper and lower accumulations of the energy output/demand in any time period $[s, t]$ $(0 \leq s \leq t)$ as shown in Fig. 1. Therefore, according to the stochastic energy network calculus theory, the uncertainty power output and load demand can be expressed as follows,

$$\left\{ \begin{array}{l} \Pr \left\{ \sup_{0 \leq s \leq t} \left[S(s,t) - \beta_s^u(t-s) \right] > x \right\} \leq \varepsilon_s^u(x) \\ \Pr \left\{ \sup_{0 \leq s \leq t} \left[\beta_s^l(t-s) - S(s,t) \right] > x \right\} \leq \varepsilon_s^l(x) \end{array} \right. \quad (1)$$
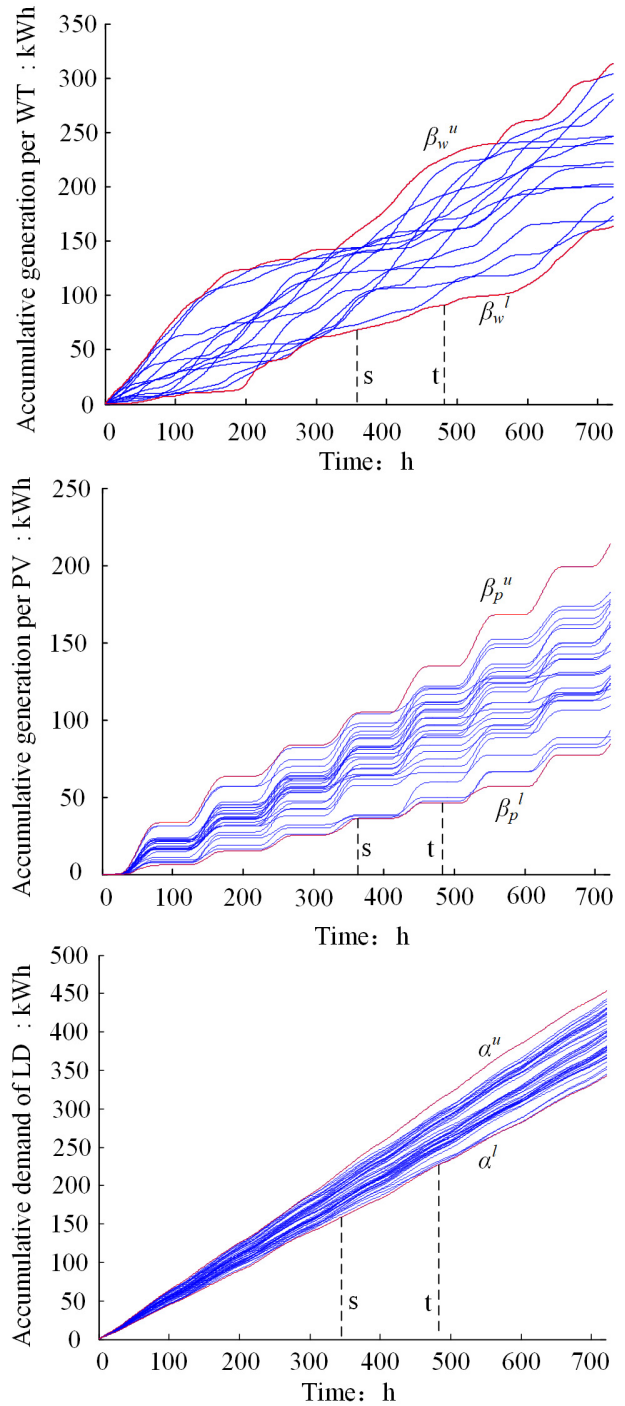

FIGURE 1. Cumulative energy envelope characterization under source-load random uncertainty.

$$\left\{ \begin{array}{l} \Pr \left\{ \sup_{0 \leq s \leq t} \left[D(s,t) - \alpha^u(t-s) \right] > x \right\} \leq \varepsilon_d^u(x) \\ \Pr \left\{ \sup_{0 \leq s \leq t} \left[\alpha^l(t-s) - D(s,t) \right] > x \right\} \leq \varepsilon_d^l(x) \end{array} \right. \quad (2)$$

where (1) is the intermittent power output description model and (2) is the load demand description model. $\varepsilon_s^u(x)$ and

$\varepsilon_s^l(x)$ represent the boundary functions of the upper and lower limits of the uncertainty power output, respectively. $\varepsilon_d^u(x)$ and $\varepsilon_d^l(x)$ represent the boundary functions of the random upper and lower bound curves of the power demand, respectively. Sup[x] represents the operation used to find the bounds of the set, and $S(s, t)$ represents the cumulative energy of the uncertainty power supply in the period [s, t].

In particular, when considering the simultaneous planning of a controllable power supply, the energy deficit in the planned area can be characterized as follows,

$$L(t) = [D(s, t) - S(s, t) - M(t)]^+ \quad (3)$$

where $M(t)$ represents the cumulative amount of energy of the controllable power supply during the period [0, t] and $[x]^+ = \max\{x, 0\}$.

The loss-of-energy probability (LOEP) can be characterized by (4). To ensure the energy balance in the planned area, it is necessary to meet the constraints of (5),

$$\Pr\{L(t) \geq x\} \leq \varepsilon_s^u \otimes \varepsilon_d^l$$
$$\left(x + M(t) - \sup_{0 \leq s \leq t} \left[\beta^u(s) - \alpha^l(s) \right] \right) \quad (4)$$
$$\sup_{0 \leq s \leq t} \{\Pr\{L(t) \geq 0\}\} \leq \alpha^*(t) \quad (5)$$

where $\Pr\{L(t) > x\}$ represents the LOEP index; $\alpha * (t)$ represents the horizon LOEP index, which in this paper, takes the value of 0.1.

B. SHORT-TIMESCALE SOURCE-LOAD PREDICTION ERROR UNCERTAINTY MODEL

To accurately characterize the uncertainty of source-load prediction errors, a box interval model is constructed, as shown below, to calculate the renewable power output and load demand at time t [29],

$$\begin{cases} P_{k,t} = P_{for,k,t} + P_{dev,k,t} r_{k,t} \\ P_{dev,k,t} \in [P_{k,t,\min}, P_{k,t,\max}] \\ r_{k,t} \in [0, 1] \\ \sum_{t=1}^{T} r_{k,t} \leq N_k \end{cases} \quad (6)$$

where $P_{k,t}$ and $P_{for,k,t}$ represent the actual output/demand and predicted output/demand of the uncertain source k at time t; respectively; $P_{dev,k,t}$ is the deviation between the actual values and the predicted values; and $P_{k,t,max}$ and $P_{k,t,min}$ are the upper and lower bounds of the deviation range of uncertainty source k, respectively. Because there is a significant difference between the source and load prediction accuracies, the prediction errors of WT and PV outputs are less than 30%, and the load demand prediction errors are less than 10%. Therefore, the prediction error bands of the source and load can be characterized by the different upper and lower bounds with respect to their prediction errors. In addition, to prevent a conservative microgrid capacity optimization

scheme, this paper selects a coordination factor $r_{k,t}$ to characterize the uncertainty of the source and load prediction error, where N_k denotes the uncertainty degree of the simulation scenario for the uncertain source k.

To simplify the calculations in this paper, the Monte Carlo method is applied to investigate the uncertainty of the source and load prediction errors of the isolated microgrid under the aforementioned constraints of prediction error uncertainty.

III. LOAD CHARACTERISTIC MODELING UNDER LDM
In this paper, loads are classified into three categories according to their controllability: interruptible loads, shiftable loads and uncontrollable loads. The descriptions and models of each category are as follows.

A. INTERRUPTIBLE LOAD
We can schedule the interruptible load to be interrupted during any contract period based on power management requirements, but the capacity and duration of each interruption cannot exceed the contracted interruption capacity or upper duration limit. It is assumed that the load can be rescheduled within one scheduling period (i.e., 24 h), but the interval between the two scheduling steps cannot be less than the contracted scheduling interval. Thus, the interruptible load model should satisfy the following constraints.

1) LOAD POWER CONSTRAINT

$$\begin{cases} \sum_{t \in H_{IL}} P_L(t) \leq \sum_{j \in A} N_j P_j \mathrm{U}(t) + \sum_{t \in H_{IL}} P_{NCL}(t) \\ P_L(t) \geq P_{NCL}(t), \quad t \in T \\ P_L(t) = P_{NCL}(t), \quad t \notin H_{IL} \end{cases} \quad (7)$$

where H_{IL} represents the set of interruptible time periods, which is a set of multiple time periods; N_j represents the number of interruptible devices of class j; P_j represents the active power of a class j interruptible device; $P_{NCL}(t)$ represents the uncontrollable load power; and U(t) is a binary decision variable that indicates whether the contract management response is executed at the sampling point t.

2) MAXIMUM INTERRUPT DURATION CONSTRAINT

$$\max_{\forall s \in H_{IL}} \left\{ \left(V_{j,s,\bar{t}} - V_{j,s,\underline{t}} \right) \Delta t, T_{j,IL,\max} \right\} \leq T_{j,IL,\max} \quad (8)$$

where S represents a contiguous subset of the interruptible period set H_{IL}; $V_{j,s,\bar{t}}$ and $V_{j,s,\underline{t}}$ indicate the final sampling point and the beginning sampling point of the interruption in the continuous subset S, respectively; Δt represents the time step of the sampling point; and $T_{j,IL,max}$ represents the maximum interruption duration for the j_{th} type of interruptible devices.

3) MINIMUM SCHEDULING INTERVAL DURATION CONSTRAINT

$$\min_{\forall k \in (T - H_{IL})} \left\{ \left(V_{j,k,\bar{t}} - V_{j,k,\underline{t}} \right) \Delta t, T_{j,IL,\min} \right\} \geq T_{j,IL,\min} \quad (9)$$

Equation (6) indicates that for a continuous subset k of any unscheduled time period set (T-HIL), the scheduling period duration between the maximum and minimum sampling points satisfies the minimum scheduling interval duration constraint.

B. SHIFTABLE LOAD

For shiftable loads, the entire scheduling period T can be divided into different periods:

$$T = H_i \cup H_n \cup H_m \qquad (10)$$

where H_i represents a shiftable time window, indicating that the shiftable device can be scheduled during this time period; H_n represents the ordinary operation period of the shiftable device; and H_m indicates the time period in which the load is not allowed to participate in shifting scheduling. The shiftable loads must satisfy the following constraints.

1) LOAD POWER CONSTRAINT

$$
\begin{cases}
P_L(t) \geq P_{NCL}(t), \; t \in T \\
P_L(t) = P_{NCL}(t), \; t \in H_m \\
\begin{cases}
\sum\limits_{t \in H_i} P_L(t) \geq \sum\limits_{j \in A} N_j P_j D_j F_{i,j} \mathrm{U}(t) + \sum\limits_{t \in H_i} P_{NCL}(t) \\
F_{i,j} = 1 - \min \left\{ \dfrac{G_j}{D_j}, 1 \right\} \\
G_j = \min \left\{ D_j, \left(D_j - O_{j,t} \right) \right\} \\
\end{cases} \\
\begin{cases}
\sum\limits_{t \in H_n} P_L(t) \leq \sum\limits_{j \in A} N_j P_j Z_{j,t} \mathrm{U}(t) + \sum\limits_{t \in H_n} P_{NCL}(t) \\
Z_{j,t} = \begin{cases} 1, & t \in H_n \\ 0, & t \notin H_n \end{cases}
\end{cases}
\end{cases} \qquad (11)
$$

where $P_L(t)$ represents the load power after shifting control; $P_{NCL}(t)$ represents the uncontrollable load power; (H_i/H_n) represents the remaining time in the period H_i as a fraction of period H_n; N_j represents the number of the jth type of the shiftable devices; P_j represents the active power of the jth type of the shiftable devices; D_j represents the length of use of the jth type of the shiftable devices; $F_{i,j}$ represents the conversion factor of the jth type of the shiftable devices, where $F_{i,j} \in [0, 1]$; G_j indicates that the jth type of the shiftable devices needs to continue using power at the initial time of scheduling; and $O_{j,t}$ indicates that the jth type of the shiftable devices has been used for a long duration at time t.

2) LOAD ENERGY CONSTRAINT

$$W_j = P_{j,av} \; D_j \Big|_{D_{j \in H_n}} = P_{j,av} \; D_j \Big|_{D_{j \in H_i}} \qquad (12)$$

where W_j represents the energy consumption required for the shiftable load; and $P_{j,av}$ represents the average operating power of the shiftable loads.

C. UNCONTROLLABLE LOAD

A load that is not included during regulation of the power market contract is called an uncontrollable load. This type of load primarily satisfies the rigid demands of the users. This paper uses $P_{NCL}(t)$ to represent the uncontrollable load power.

IV. CAPACITY OPTIMIZATION MODEL CONSIDERING MSUC AND LDM

In this paper, we consider a planning-operation two-layer optimization model for isolated microgrid capacity optimization. In the outer-layer planning level, considering the source-load random uncertainty, a stochastic network calculus theory is used to ensure energy balance in an isolated microgrid. The planning decision is made with the goal of minimizing investment, which mainly resolves the system energy balance. In the inner-layer operation level, the uncertainty of source-load prediction errors is considered via Monte Carlo simulations, and the power outputs of the WT, PV, CMG, and ESS are optimized with regard to the load-controllable features of LDM.

A. OUTER-LAYER OPTIMIZATION MODEL

In the two-layer optimization model proposed in this paper, the outer optimization model is utilized to solve the capacity planning problem for a microgrid, including the capacity of the WT, PV, CMG and ESS, considering the influence of source-load random uncertainty to satisfy the energy balance constraint. The decision variables of the outer-layer optimization include the capacities of the WT, PV, CMG and ESS. The objective function is the total cost of the microgrid, including the investment costs of different energy sources and the operation cost of the system. The optimization model is as follows.

1) OBJECTIVE FUNCTION

$$
\begin{cases}
\min C_{A\&O} = C_{investment} + C_{operation} \\
C_{investment} = \eta_D \cdot [C_{DRE} + C_F + C_{ESS}] \\
C_{DRE} = \eta_{pv} N_{PV} P_{PV\_unit} + \eta_{wind} N_{WT} P_{WT\_unit} \\
C_F = \eta_f N_F P_{F\_unit} \\
C_{ESS} = N_{ESS} [\eta_B B_{ESS} + \eta_P P_{ESS} + \eta_{inv} P_{ESS}] \\
C_{operation} = C_{generation} \\
\eta_D = \dfrac{d(1+d)^{y_{ESS}}}{\{365 \times [(1+d)^{y_{ESS}} - 1]\}}
\end{cases} \qquad (13)
$$

where $C_{A\&O}$ is the total cost of investment and system operation for an isolated microgrid, including $C_{investment}$ and $C_{operation}$; $C_{investment}$ is the average daily investment cost of a system comprised of WT, PV, CMG and ESS devices; η_{pv}, η_{wind}, and η_f represent the unit capacity cost of the PV, WT, and CMG, respectively, all of which include the fixed investment cost and maintenance costs; η_B is the unit energy capacity cost; η_P is the unit power capacity cost of the storage system; and η_{inv} is the inverter cost coefficient. Because the operation cost of the microgrid is calculated over one day, the investment cost should be normalized by η_D, where η_D represents the equivalent daily coefficient and d represents the discount rate. To simplify the analysis process, we select a typical unit for study. N_{PV}, N_{WT}, N_F and N_{ESS} are defined

as the decision variables, representing the number of typical units such as PV, WT, CMG and ESS. $P_{\text{PV\_unit}}$, $P_{\text{WT\_unit}}$, and $P_{\text{F\_unit}}$ indicate the rated power of typical PV, WT and CMG unit, respectively; B_{ESS} and P_{ESS} indicate the rated capacity and rated power of the ESS, respectively.

2) RESTRICTIONS

a: INVESTMENT LIMIT CONSTRAINT

The upper bound constraint on investment in the planning area is shown as

$$0 \le C_{\text{investment}} \le \overline{C_{\text{investment}}} \qquad (14)$$

b: INSTALLED NUMBER CONSTRAINT

Due to the limited installable area, the upper limit constraint on the number of installed WT and PV units can be expressed as

$$\begin{cases} N_{\text{PV}} \le \overline{N_{\text{PV}}} \\ N_{\text{WT}} \le \overline{N_{\text{WT}}} \end{cases} \qquad (15)$$

c: ENERGY BALANCE CONSTRAINT

A planned isolated microgrid system in this paper contains PV, WT and CMG, whose numbers are N_{PV}, N_{WT}, and N_F, respectively. When considering the source-load random uncertainty, the planning scheme needs to meet the energy balance constraints. In [26], it is assumed that the minimum envelope curve for each unit energy supply satisfies $S_n \sim (\varepsilon_n^l, \beta_n^l)$, $(n = 1, 2, \ldots, N)$, and then the lowest envelope curve of the energy supply side of the combined power supply is characterized as $S \sim (\varepsilon_{combined}^l, \beta_{combined}^l)$, which satisfies the following relationship,

$$\begin{cases} \beta_{combined}^l(t) = \beta_1^l(t) + \beta_2^l(t) + \ldots + \beta_N^l(t) \\ \varepsilon_{combined}^l(x) = \varepsilon_1^l(x) \otimes \varepsilon_2^l(x) \otimes \ldots \otimes \varepsilon_N^l(x) \end{cases} \qquad (16)$$

As in the analysis process in Section II, we can obtain the energy balance constraint which include the combined power supply as follows,

$$\Pr\{L(t) \ge x\} \le \varepsilon_{s\_combined}^u \otimes \varepsilon_{d\_combined}^l$$

$$\left(x + M_{combined}(t) - \sup_{0 \le s \le t} \left[\beta_{combined}^u(s) - \alpha_{combined}^l(s) \right] \right)$$

$$\le \alpha^*(t) \qquad (17)$$

where $\varepsilon_{s\_combined}^u$ represents the boundary function of the upper limits of the uncertainty combined power output; $\varepsilon_{d\_combined}^l$ represents the boundary function of the random lower bound curves of the combined power demand; $\beta_{combined}^u(s)$ represents the upper bounds of the cumulative output of combined uncertainty sources during the statistical period; and $\alpha_{combined}^l(s)$ represents the lower bounds of the cumulative combined load demand during the statistical period.

B. INNER-LAYER OPTIMIZATION MODEL

While considering the long-term random uncertainty of the source and load, the outer-layer optimization model determines the installed capacities of different energy sources in the isolated microgrid based on the energy balance. Following this step, the inner-layer optimization model considers the short-term source-load prediction power uncertainty, and Monte Carlo simulations are performed to obtain random scenarios to address the power balance problem at the operation level. Therefore, the inner-layer optimization in this paper is essentially a simplified unit commitment (UC) problem considering the power distribution of different units on a given scheduling timescale (usually 1 h). The decision variables of the inner-layer optimization are the power outputs of the different units. The mathematical model of the inner-layer optimization is shown below.

1) OPERATION COST

$$\begin{cases} C_{\text{operation}} = C_f + C_R + C_{DR} \\ C_f = \sum_{t=1}^{T} (a_i P_{i,t}^2 + b_i P_{i,t} + c_i), \ i \in F \\ C_R = \eta_D C_{ESS}[(\sum_{t=1}^{T} |P_{ESS,t}| \Delta t)/(2N_{rep}N_{ESS}B_{ESS})] \\ C_{DR} = \sum_{t=1}^{T} \sum_{k \in K} c_{IL,k} * P_{IL,k}(t) * \Delta t \\ \qquad + \sum_{t=1}^{T} \sum_{j \in J} c_{SL,j} P_{SL,j}(t) \Delta t \end{cases} \qquad (18)$$

where $C_{\text{operation}}$ is the expected daily operation cost, which includes three terms, namely C_f, C_R, and C_{DR}. C_f is the CMG operation cost, which is related to the cost coefficients a_i, b_i, and c_i. C_R is the replacement cost of the ESS. Since the ESS will gradually age due to frequent charging and discharging processes, its lifetime can be calculated based on the cumulative transferred energy [30]. $\sum_{t=1}^{T} |P_{ESS,t}| \Delta t$ expresses the cumulative transferred energy for the storage system, N_{rep} is the rated cycle number, and $2N_{rep}N_{ESS}B_{ESS}$ is the expected total transfer energy for the life cycle.

$[(\sum_{t=1}^{T} |P_{ESS,t}| \Delta t)/(2N_{rep}N_{ESS}B_{ESS})] \in [0, 1]$ indicates the life status of the storage. When the value is 1, the storage system has reached the end of its life. C_{DR} represents the subsidy cost of the LDM in the microgrid, where K represents the interruptible load set; $c_{IL,k}$ represents the kth subsidy unit price (¥/kW) under interruptible load management; $P_{ILk}(t)$ represents the interruption capacity of the kth class of interruptible loads during the tth scheduling period; J is the shiftable load set; $c_{SL,j}$ represents the scheduling cost of the jth type of the shiftable load (¥/kW); $P_{SL,j}(t)$ is the shift capacity of the jth type of the shiftable loads during the

t_{th} scheduling period; and Δt represents the scheduling time interval, which is taken as 1 h.

2) RESTRICTIONS
a: POWER BALANCE CONSTRAINT
At the operation level, considering the impact of LDM in a random scenario, the source and load must satisfy the power balance constraints described in the following equation.

$$P_{s,DRE,t} + P_{s,i,t} + P_{s,ESS,t} = P_{s,L,t} \qquad (19)$$

b: WT AND PV ABANDONMENT CONSTRAINTS
During operation of the isolated microgrid, due to the uncertainty and randomness of wind and solar energy, the power curtailment of WT and PV must be considered to ensure instantaneous power balance. The relevant model is detailed in Section IV-*C* below.

$$R_{s,Ab} \leq \overline{R_{Ab}} \qquad (20)$$

c: UNIT OUTPUT LIMIT CONSTRAINT
The maximum power limits of WT, PV, CMG and ESS units are shown as

$$\begin{cases} \underline{P_{s,i}} \leq P_{s,i,t} \leq \overline{P_{s,i}} \\ \underline{P_{s,DER}} \leq P_{s,DER,t} \leq \overline{P_{s,DER}} \\ \underline{P_{s,ESS}} \leq P_{s,ESS,t} \leq \overline{P_{s,ESS}} \end{cases} \qquad (21)$$

d: ESS OPERATION CONSTRAINTS

$$\begin{cases} B_{s,ESS}SOC_{s,ESS,t} = \begin{cases} B_{s,ESS}SOC_{s,ESS,(t-1)} + \Delta t P_{s,ESS,t}\eta_c, \\ \quad \text{if } P_{s,ESS,t} \geq 0 \\ B_{s,ESS}SOC_{s,ESS,(t-1)} - \Delta t P_{s,ESS,t}/\eta_d, \\ \quad \text{if } P_{s,ESS,t} < 0 \end{cases} \end{cases}$$

$$(22)$$

$$\begin{cases} \underline{SOC_{s,ESS}} \leq SOC_{s,ESS,t} \leq \overline{SOC_{s,ESS}} \\ SOC_{s,ESS,0} = SOC_{s,ESS,T} \end{cases} \qquad (23)$$

e: LDM CONSTRAINT

$$f\left(P_{s,L,t}\right) \geq 0 \qquad (24)$$

where (24) is a compact form of the LDM constraint. A detailed description has been given in Section III.

C. WIND AND SOLAR ENERGY CURTAILMENT OF ISOLATED MICROGRID
Rational planning for the capacity of WT, PV, CMG and ESS units is necessary to solve the power curtailment of WT and PV. In this paper, we use the concept of energy conservation over a complete scheduling period T of the microgrid in a scenario to analyze the curtailed energy during operation of

the microgrid.

$$\begin{cases} E_{G,T,s\in S} = \sum_{t=1}^{T}\left(P_{PV,s,t}t + P_{WT,s,t}t\right) \\ E_{load,T,s\in S} = \sum_{t=1}^{T}\left(P_{LD,s,t}t\right) \\ E_{F,T,s\in S} = \sum_{t=1}^{T}\left(P_{f,s,t}t\right) \\ E_{IL,T,s\in S} = \sum_{t=1}^{T}\left(P_{IL,s,t}t\right) \\ E_{C,T,s\in S} = E_{load,T,s\in S} - E_{F,T,s\in S} - E_{IL,T,s\in S} \\ E_{AWAV,T} = E_{G,T,s\in S} - E_{C,T,s\in S} \end{cases} \qquad (25)$$

where $E_{G,T,s\in S}$ represents the total power generation of the DRE during scheduling period T; $P_{PV,s,t}$ and $P_{WT,s,t}$, respectively; represent the actual power generation of the PV and WT for scenario s (unlimited power output); $E_{load,T,s\in S}$ represents the total load demand during the dispatch period T (not considering LDM); $E_{F,T,s\in S}$ represents the total power generation of the CMG within the scheduled time period T; $E_{IL,T,s\in S}$ represents the total interrupted power of the interruptible load during the dispatch period T under LDM conditions; $E_{C,T}$ represents the actual consumption of renewable energy; and $E_{AWAV,T}$ represents the total amount of curtailed energy. Thus, the energy curtailment rate R_{Ab} is defined as shown below and satisfies the following constraints:

$$\begin{cases} R_{Ab} = E_{AWAV,T,s\in S}/E_{G,T,s\in S} \\ R_{Ab} \leq R_{Ab}^{\max} \end{cases} \qquad (26)$$

where $R_{Ab}^{\max}$ indicates the upper limit of the curtailment rate.

V. SOLUTION OF THE MODEL
A. THE SOLVING FLOW CHART OF THE MODEL
Fig. 2 shows the calculation flow of the capacity optimization model considering MSUC and LDM. The flow chart includes four main modules: the source-load random energy processing module, the outer planning module, the inner-layer operation module and load modification module.

B. MODEL LINEARIZATION
The two-layer optimization model proposed in this paper employs MILP, which is solved using the YALMIP toolbox and CPLEX solver. The model returns decision variables including N_{PV}, N_{WT}, N_F and N_{ESS}, as well as different types of power supplies and energy storage dispatch decision at each time t.

1) CMG OPERATION COST LINEARIZATION
Equation (18) shows that the relationship between the operation cost and the CMG power supply is nonlinear. This paper replaces the above nonlinear model with a piecewise linear
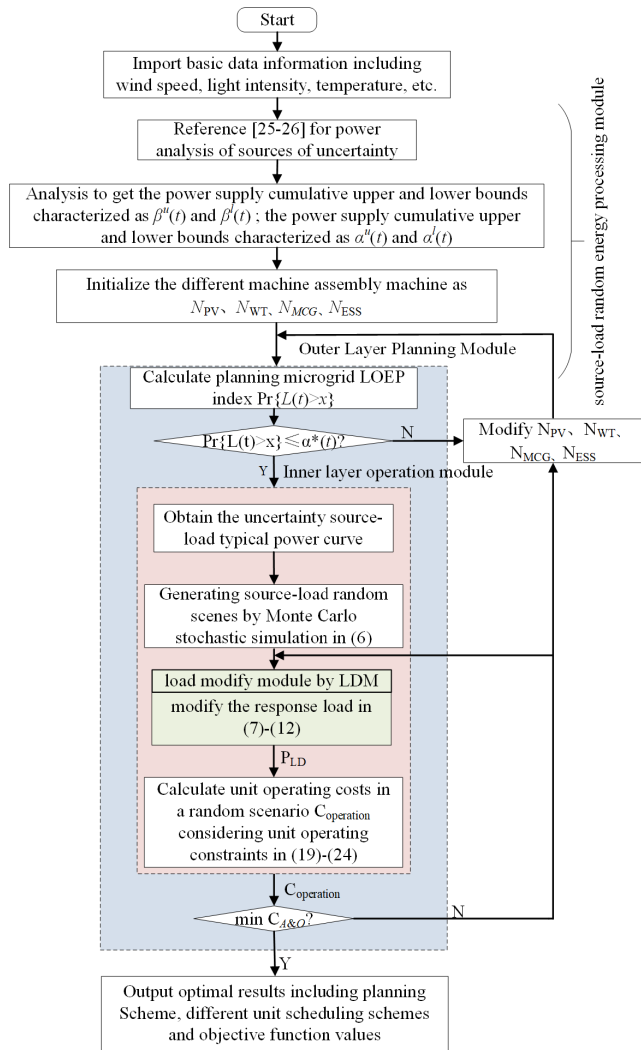
FIGURE 2. The calculation flow of the capacity optimization model considering MSUC and LDM.

interpolation function $\varphi_h(P_{i,t})$ in [31].

$$
\begin{cases}
h = \dfrac{\overline{P_i} - \underline{P_i}}{n}, \ i \in F \\
P_i^j = \underline{P_i} + jh, \ j = 0, 1, \ldots, n \\
\varphi_h(P_{i,t}) = \left(P_{i,t} - P_i^j\right)\left[a_i\left(P_i^{j+1} - P_i^j\right) + b_i\right] \\
\qquad\qquad + C_f^j, P_{i,t} \in \left[P_i^j, P_i^{j+1}\right] \\
C_f^j = a_i\left(P_i^j\right)^2 + b_i P_i^j + c_i
\end{cases}
\tag{27}
$$

where h ensures that the CMG power output range is equally divided by n and $\varphi_h(P_{i,t})$ represents a linear interpolation function for a segmentation interval $\left[P_i^j, P_i^{j+1}\right]$. Particularly, the error estimated by the above piecewise linear interpolation function satisfies the following constraints,

$$
\begin{cases}
M = \max_{\underline{P_i} \le P_{i,t} \le \overline{P_i}} \left|C_f''\right| \\
\left|R\left(P_{i,t}\right)\right| = \left|C_f\left(P_{i,t}\right) - \varphi_h\left(P_{i,t}\right)\right| \le \dfrac{M}{8}h^2, \\
\qquad\qquad \forall P_{i,t} \in \left[\underline{P_i}, \overline{P_i}\right]
\end{cases}
\tag{28}
$$

2) LINEARIZATION OF LDM CONSTRAINTS

For the LDM constraints, each sampling point takes the value of a binary decision variable, 0 or 1, depending on whether contract management is performed, which is represented as U(t). The actual response power for each sampling point is $N_{CL}P_{CL\_unit}$U(t), where N_{CL} represents the number of controllable loads and P_{CL_unit} represents the power of a single-unit controllable load. Consequently, there is inevitably a nonlinear constraint, which is the product of the integer decision variable N_{CL} and the binary variable U(t). To linearize the constraint, we first assume that N_{CL} has a large upper limit, which is set to N_{CL_max}, and add two temporary variables, Q(t) and R(t).

Then, the above nonlinear constraints can be linearized as follows,

$$
\begin{cases}
R(t) \le (1 - U(t)) \cdot N_{CL\_\max} \\
Q(t) = N_{CL}(t) - R(t) \\
Q(t) \le N_{CL} \cdot U(t)
\end{cases}
\tag{29}
$$

Thus, $Q(t)$ can be used to replace N_{CL}U(t) for nonlinear problems.

VI. CASE ANALYSIS

To verify the rationality and effectiveness of the proposed model and method, a typical microgrid is taken as an example to study the capacity optimization problem including the WT, PV, CMG and ESS. In the outer-layer planning level, our model considers a planning horizon of 20 years. In the inner-layer of the scheduling model, we selected 64 scenarios throughout the year to analyze the operation and scheduling of different types of units. These scenarios generated from different 4 seasons can sufficiently cover the characteristics of the annual load demand and renewable resource supply [32].

A. PARAMETER SETTINGS

Table 1 summarizes the technical and economic parameters of the isolated microgrid, as well as other parameters considered in the study examples [32]. Tables 2 and 3 present typical load data for demand management contracts in the region [17]. Fig. 3 shows the monthly average ambient temperature, daily radiation intensity, and wind speed in the planning area, and the required meteorology data are provided from the meteorology site (see Refs. [33]).

B. MULTISCALE UNCERTAINTY IMPACT ANALYSIS

To briefly illustrate the processing of source and load uncertainty, we take wind power as an example, the results of which are shown in Fig.4 and 5. Fig. 4 shows the upper and lower envelopes of the source-load random uncertainty obtained by network calculus theory, solving source-load stochastic uncertainty over a long-timescale. Fig. 5 shows the random scenario with the source-charge prediction error uncertainty under the box interval constraint using Monte Carlo simulation, to solve the power operation analysis.

TABLE 1. Technical and economic parameters for microgrid components.

ECONOMIC PARAMETERS			
c_IL	¥0.8/ kWh	$\overline{C_{investment}}$	¥50000
c_SL	¥0.5/ kWh	r	0.06
Life_PV & Life_WT	20 years	Planning	20 years
PV MODULE TECHNICAL PARAMETERS			
P_{PV_unit}	1 kW	C_PV	¥9000/ kW
M_PV	¥750/ kW	G_{STC}	1 kWh/m²
T_{STC}	25°C	k	0.004~0.006
WIND MODULE TECHNICAL PARAMETERS			
P_{WT_unit}	1 kW	C_WIND	¥7200/ kW
M_WIND	¥500/ kW	v_{ci} & v_{co} & v_r	2.1 m/s & 20 m/s & 9 m/s
CMG MODULE TECHNICAL PARAMETERS			
P_{F_unit}	5kW	C_F	¥1500/ kW
M_F	¥500/ kW	c_fule	¥1.68/ kW
ENERGY STORAGE BATTERY MODULE TECHNICAL PARAMETERS			
P_{ESS}	1.2kW	B_{ESS}	3 kWh
M_ESS	¥750/ kW	C_PESS	¥1085/ kW
C_I	¥1380/ kW	$SOC_{ESS,0}$	0.6
SOC_{ESS}^{min} & SOC_{ESS}^{max}	0.1 & 0.9	η_c	0.9
η_d	0.9	N_{rep}	1500

TABLE 2. Shiftable load technical parameters.

Equipment type	washer	dryer	dishwasher	EV
Number of schedules	10	10	10	10
P (kW)	0.5	1	0.9	5
Duration (h)	1	1	1	3
H_i	[7:00-24:00]	[7:00-24:00]	[18:00-24:00]	[0:00-24:00]
H_n	[7:00-24:00]	[7:00-24:00]	[18:00-20:00]	[19:00-21:00]
H_m	[0:00-7:00]	[0:00-7:00]	[0:00-18:00]	-

TABLE 3. Interruptible load technical parameters.

Equipment type	N_j	P_j (kW)	$N_{j,IL}$	$T_{j,IL,max}$	$T_{j,IL,min}$
air conditioner	10	1.5	3	1	2
water heater	10	3	3	2	2

Due to uncertainty in the source and load power, to prevent a conservative microgrid capacity optimization scheme, different coordination factors $r_{k,t}$ and N_k are set, and the results of system planning under different uncertainty degrees are analyzed. The relevant results are shown below in Table 4.

From Table 4, we can see that the total investment operating cost of the system increases as the source-load uncertainty increases. In addition, Table 4 shows that as the degree of source and load uncertainty increases, the investment in controllable resources (CMG and ESS) to handle system uncertainty will increase (the column of investment in controllable resources), resulting in higher system planning costs. Similarly, when the degree of source and load
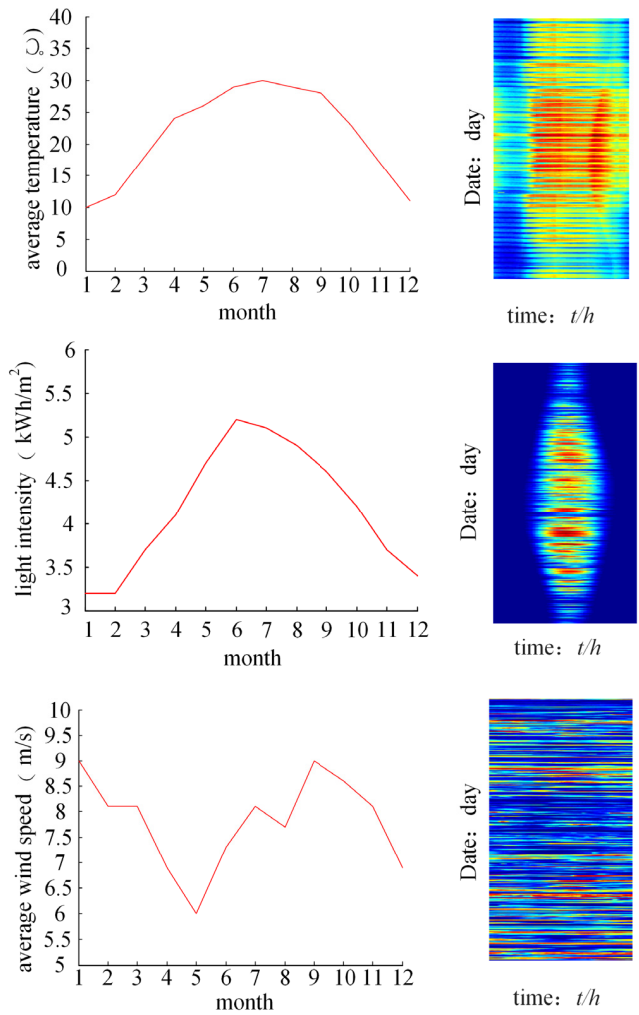
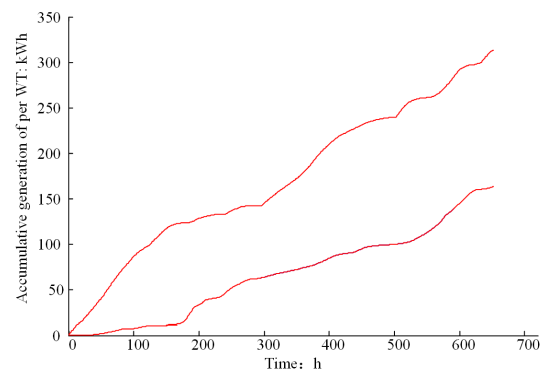**FIGURE 3.** Monthly average temperature/light intensity/wind speed in the planned area.

FIGURE 4. Long-term wind random uncertainty.

uncertainty is low, the installed capacity of the system uncertainty resources (WT and PV) is higher (the column of investment in uncertainty resources), and the cost of dealing with the source and load uncertainty is lower (the column of operation cost).

TABLE 4. Analysis of planning results with msuc.

Cases	WT/Num	PV/Num	CMG/Num	ESS/Num	Investment in controllable resources/10^4¥	Investment in uncertainty resources/10^4¥	Operation cost/10^4¥	$C_{A\&O}$/10^4¥
$r_{k,t}=0$	3373	444	274	61	0.07	0.72	0.31	1.10
$r_{k,t}=1;N_k=6$	3289	426	254	150	0.09	0.70	0.34	1.13
$r_{k,t}=1;N_k=12$	2784	307	256	246	0.12	0.58	0.48	1.18
$r_{k,t}=1;N_k=24$	2654	289	264	278	0.13	0.56	0.53	1.21
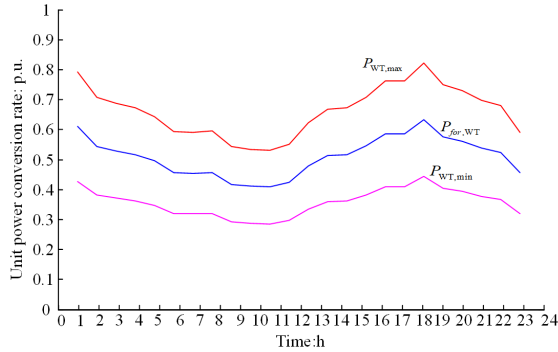
FIGURE 5. Short-term wind power prediction error uncertainty.

C. LDM IMPACT ANALYSIS

1) LDM IMPACT WITH THE SAME UNCERTAINTY DEGREE

For a given source and load uncertainty ($r_{k,t} = 1$; $N_k = 12$) and considering the role of LDM during operation, the results of capacity planning are analyzed and optimization results are shown in Table 5 below.

TABLE 5. Impact analysis of ldm on capacity planning.

Cases	WT/Num	PV/Num	CMG/Num	ESS/Num	$C_{A\&O}$/10^4¥
NLDM	2784	307	256	246	1.18
LDM	2855	115	257	214	1.09

Table 5 shows that when considering LDM, the installed capacity of the WTs does not decrease, but rises instead. This result occurs because LDM can adjust the user-side load characteristics to adapt to changes in the WT output, reducing the power curtailment of WT and the dependence on energy storage equipment. It can be seen from Table 5 that before and after LDM, the cost of energy storage equipment is significantly reduced, and the system planning investment cost is reduced. This result occurs because LDM can achieve the same effect (energy time and space migration) as energy storage equipment to a certain extent by controlling the interruptible and shiftable loads, thereby reducing the installed capacity of energy storage equipment. At present, the high cost of energy storage is the primary factor affecting the planning investment cost. Therefore, reducing the investment in energy storage equipment will directly reduce the total investment cost of the system.

For the same scenario (typical source and load curve), we consider the inclusion of LDM to analyze the output of

different types of power supplies during operation and discuss the impact of LDM on capacity planning in detail. Analysis results of the source and load power balance during operation for a given scenario are shown in Fig. 6 and 7.
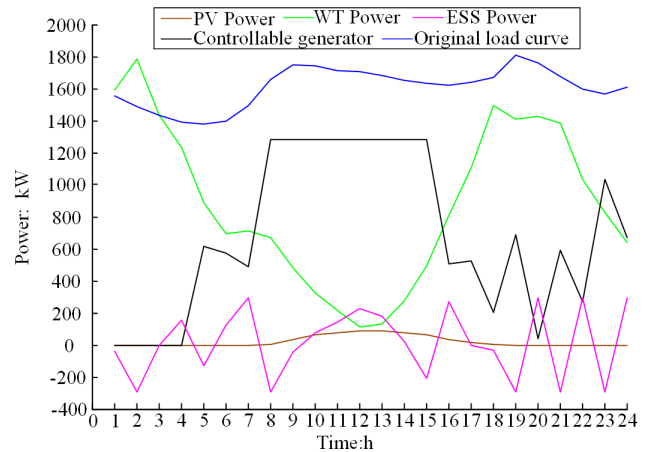

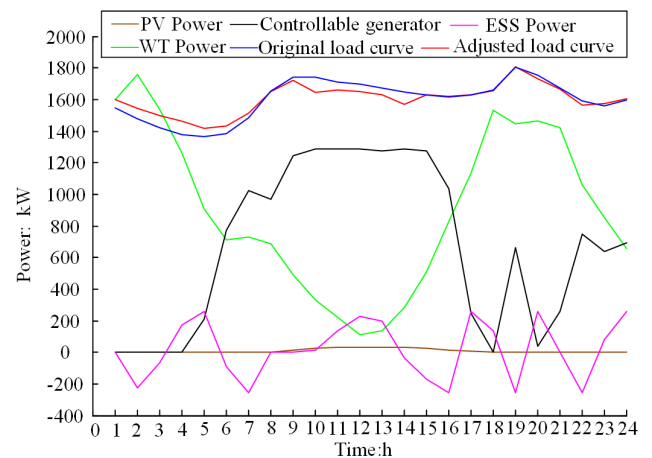**FIGURE 6.** Source-load power balance analysis without LDM under case 1.

FIGURE 7. Source-load power balance analysis with LDM under case 1.

After simulating the typical source-load data sets in different scenarios throughout the year and obtaining the expected results, Fig. 6 and Fig. 7 show the scheduling operations of different types of units in one day without LDM and with LDM, respectively.

From Fig. 6 and Fig. 7, it can be seen that under the influence of the same degree of uncertainty, LDM can effectively

reduce the frequency of charge and discharge of the ESS from 8 a.m. to 11 a.m. and reduce the amount of exchanged energy. Meantime, LDM can also reduce the need for controllable power dispatch frequencies and the frequency of ramp-up and rump-down (i.e., 5-10 and 18-24), and reduce the difficulty of scheduling operation control.

As shown in Fig. 7, the points in this curve (i.e., 1-7 and 9-15) represent that the controllable load will adjust the load characteristics as the renewable energy output increases and decreases.

2) LDM IMPACT WITH DIFFERENT UNCERTAINTY DEGREES

To comprehensively analyze the degree of system uncertainty and the influence of LDM in the model, we analyze the results from different dimensions (system uncertainty and LDM) and set two cases which are summarized in Table 6. Fig. 8 and Fig. 9 present the scheduling operation of different types of units under Case 2, whereas the scheduling results of Case 1 have already been shown in Fig. 6 and Fig. 7.
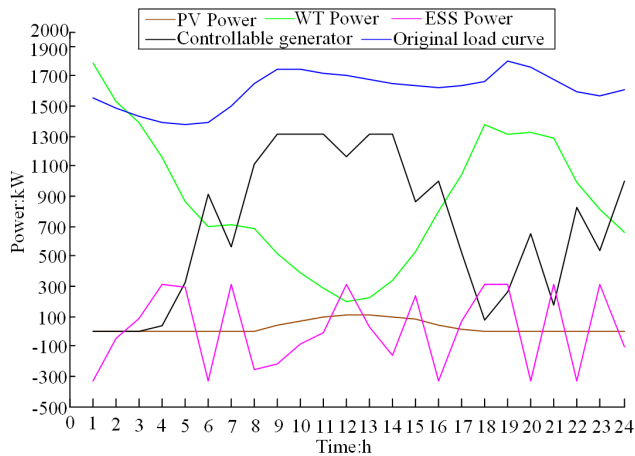

FIGURE 8. Source-load power balance analysis without LDM under case 2.

From Fig. 6 and Fig. 8, we can see that as the degree of system uncertainty increases, the scheduling and control of controllable resources (CMG and ESS) become more frequent and dependent (i.e., 4-8 and 15-24 in Fig. 8). From Fig. 8 and Fig. 9, we can see that under the influence of the same degree of uncertainty, LDM can significantly reduce the system's requirements for controllable power supply and energy storage equipment operation control scheduling (i.e., 7-16 and 18-24).

Upon comparing the influence of different types of unit dispatching operation results under different simulation cases (the different degrees of uncertainty and whether the LDM participates), the main results include the controllable power supply, energy storage equipment and renewable energy consumption, etc.; and are shown in Table 6.

Table 6 shows that LDM can improve the load profile. For example, the minimum load factor increased by 0.02 compared to the original load curve (from the case of $r_{k,t} = 1$;
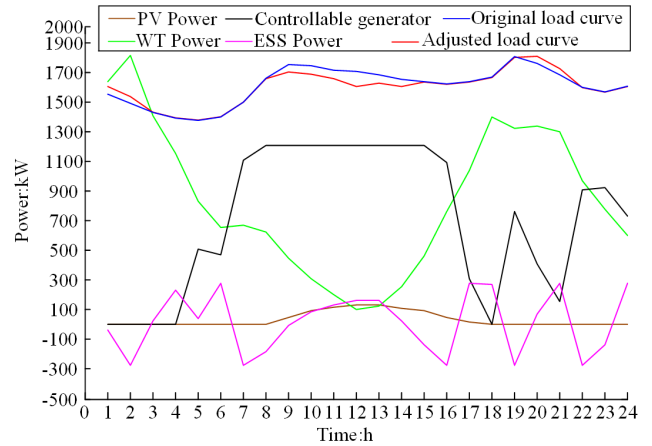

FIGURE 9. Source-load power balance analysis with LDM under case 2.

TABLE 6. Result analysis for a specific operation scenario.

Cases		Controllable power ratio	R_{Ab}	Energy storage equipment transfer energy /kWh	Minimum load factor
1 ($r_{k,t}$=1; N_k=12)	w/o LDM	42.6%	3.73%	2147.3	0.76
	w/ LDM	42.2%	3.93%	1799.5	0.78
2 ($r_{k,t}$=1; N_k=24)	w/o LDM	46.7%	2.19%	2896.5	0.76
	w/ LDM	44.3%	2.01%	2086.6	0.76

$N_k = 12$). Otherwise, LDM has the same effect as the energy storage device to some extent (namely, peak-load shifting). For a period of one day, the transferred energy of the ESS was reduced (by approximately 348 kWh in case one; by approximately 810 kWh in case two), and thus, the service life of the energy storage equipment can be effectively extended. Furthermore, as the degree of uncertainty increases (no matter whether LDM is considered), the controllable power ratio and the exchanged power of the ESS significantly increase.

In addition, the potential effect of LDM was analyzed for an interruptible load (2%) and a shiftable load (3%). According to [34], with the development of technology and market mechanisms, the demand-side response potential can reach 20%. Therefore, for microgrid planning, substantial potential remains for the load side.

D. DISCUSSION OF WIND AND SOLAR ENERGY CURTAILMENT

For isolated microgrid planning, it is necessary to discuss the energy curtailment of WT and PV to meet the requirements of national planning and microgrid construction, rather than blindly building and developing DRE. The analysis results are shown in Table 7 below.

Table 7 shows that limiting the curtailment of wind and solar energy will directly lead to increased system investment costs. For the same curtailment, compared with the NLDM

TABLE 7. Analysis of the influence of different abandoned wind and solar energy restrictions on system planning.

R_{Ab}	LDM	WT/Num	PV/Num	CMG/Num	ESS/Num	$C_{A\&O}/10^4$¥
≤20%	Yes	2855	115	257	214	1.09
	No	2784	307	256	246	1.18
≤15%	Yes	2709	352	254	247	1.24
	No	2658	354	284	263	1.28

case, LDM can adapt to the renewable energy output by adjusting the load characteristics, thus increasing the installed capacity of renewable energy and the penetration rate of new energy and reducing the dependence on energy storage equipment.

In summary, by using configuration optimization and considering the influence of MSUC with increasing uncertainty, the installed capacity of controllable resources (CMG and energy storage) will increase accordingly to ensure long-term energy balance and short-term power balance. After LDM is adopted at the operation level, the installed capacity of renewable energy is reduced due to the adjustment of load-side characteristics by the LDM to adapt to the new energy output. Moreover, the transfer power of the energy storage equipment is reduced, and its lifetime is increased.

VII. CONCLUSION

To optimize the capacity of an isolated microgrid, this paper establishes a microgrid capacity optimization model considering LDM and MSUC. The main conclusions are as follows:

- Source and load uncertainty have a substantial impact on isolated microgrid planning. When the source and load uncertainty is low, the installed capacity of the system's uncertain resources (WT and PV) is higher, and the source-load uncertainty cost is lower. When the source and load uncertainty increases, the investment in controllable resources (CMG and ESS) required for system uncertainty will increase, resulting in higher system planning costs.
- At the operational level, by introducing LDM, the user-side load demand characteristics can be adjusted to adapt to changes in renewable energy output, reducing the curtailment of wind and solar energy and the dependence on energy storage equipment. In addition, by controlling the interruptible and shiftable loads, LDM can perform the same function as that of the ESS (peak-load shifting), thereby reducing the transfer energy of the ESS and prolonging its service life.
- This paper is conservative in its discussion of LDM. Further study is needed regarding the potential of LDM, with detailed modeling of the operation characteristics, response characteristics and price elasticity of the load-side power equipment, to fully enable LDM use in instantaneous power balance and to provide guidance for the planning and operation of microgrids.
- Low computational efficiency is a drawback of the existing MILP-based algorithms used for this paper. In next

step, we are going to modify our bi-level model via a decomposition-coordination optimization framework to improve its efficiency and maintain accuracy of the proposed model.

REFERENCES

[1] S. Parhizi, H. Lotfi, A. Khodaei, and S. Bahramirad, "State of the art in research on microgrids: A review," *IEEE Access*, vol. 3, pp. 890–925, 2015.

[2] H. Xie, S. Zheng, and M. Ni, "Microgrid development in China: A method for renewable energy and energy storage capacity configuration in a megawatt-level isolated microgrid," *IEEE Electrific. Mag.*, vol. 5, no. 2, pp. 28–35, Jun. 2017.

[3] A. H. Fathima and K. Palanisamy, "Optimization in microgrids with hybrid energy systems–A review," *Renew. Sustain. Energy Rev.*, vol. 45, pp. 431–446, May 2015.

[4] Y. Li, Z. Yang, G. Li, D. Zhao, and W. Tian, "Optimal scheduling of an isolated microgrid with battery storage considering load and renewable generation uncertainties," *IEEE Trans. Ind. Electron.*, vol. 66, no. 2, pp. 1565–1575, Feb. 2019.

[5] M. Di Somma, G. Graditi, and P. Siano, "Optimal bidding strategy for a DER aggregator in the day-ahead market in the presence of demand flexibility," *IEEE Trans. Ind. Electron.*, vol. 66, no. 2, pp. 1509–1519, Feb. 2019.

[6] Y. Xiao, X. Wang, X. Wang, Z. Wu, and W. Liu, "The coordinated development path of renewable energy and national economy in China considering risks of electricity market and energy policy," *IEEE Trans. Ind. Informat.*, vol. 13, no. 5, pp. 2566–2575, Oct. 2017.

[7] B. Li, R. Roche, D. Paire, and A. Miraoui, "A price decision approach for multiple multi-energy-supply microgrids considering demand response," *Energy*, vol. 167, pp. 117–135, Jan. 2019.

[8] F. Kalavani, B. Mohammadi-Ivatloo, and K. Zare, "Optimal stochastic scheduling of cryogenic energy storage with wind power in the presence of a demand response program," *Renew. Energy*, vol. 130, pp. 268–280, Jan. 2019.

[9] T. Alharbi and K. Bhattacharya, "Optimal scheduling of energy resources and management of loads in isolated/islanded microgrids," *Can. J. Elect. Comput. Eng.*, vol. 40, no. 4, pp. 284–294, 2017.

[10] B. V. Solanki, A. Raghurajan, K. Bhattacharya, and C. A. Cañizare, "Including smart loads for optimal demand response in integrated energy management systems for isolated microgrids," *IEEE Trans. Smart Grid*, vol. 8, no. 4, pp. 1739–1748, Jul. 2017.

[11] H. Lotfi and A. Khodaei, "AC versus DC microgrid planning," *IEEE Trans. Smart Grid*, vol. 8, no. 1, pp. 296–304, Aug. 2015.

[12] L. Guo, W. Liu, B. Jiao, B. Hong, and C. Wang, "Multi-objective stochastic optimal planning method for stand-alone microgrid system," *IET Gener., Transmiss. Distrib.*, vol. 8, no. 7, pp. 1263–1273, Jul. 2014.

[13] M. H. S. Boloukat and A. A. Foroud, "Stochastic-based resource expansion planning for a grid-connected microgrid using interval linear programming," *Energy*, vol. 113, pp. 776–787, Oct. 2016.

[14] L. Zheng, W. Hu, Q. Lu, and Y. Min, "Optimal energy storage system allocation and operation for improving wind power penetration," *IET Gener., Transmiss. Distrib.*, vol. 9, no. 16, pp. 2672–2678, Mar. 2015.

[15] H. G. Lee, G.-G. Kim, B. G. Bhang, D. K. Kim, N. Park, and H.-K. Ahn, "Design algorithm for optimum capacity of ESS connected with PVs under the RPS program," *IEEE Access*, vol. 6, pp. 45899–45906, 2018.

[16] M. Faisal, M. A. Hannan, P. J. Ker, A. Hussain, M. B. Mansor, and F. Blaabjerg, "Review of energy storage system technologies in microgrid applications: Issues and challenges," *IEEE Access*, vol. 6, pp. 35143–35164, 2018.

[17] R. Atia and N. Yamada, "Sizing and analysis of renewable energy and battery systems in residential microgrids," *IEEE Trans. Smart Grid*, vol. 7, no. 3, pp. 1204–1213, May 2016.

[18] S. Kahrobaee, S. Asgarpoor, and W. Qiao, "Optimum sizing of distributed generation and storage capacity in smart households," *IEEE Trans. Smart Grid*, vol. 4, no. 4, pp. 1791–1801, Dec. 2013.

[19] U. Akram, M. Khalid, and S. Shafiq, "Optimal sizing of a wind/solar/battery hybrid grid-connected microgrid system," *IET Renew. Power Gener.*, vol. 12, no. 1, pp. 72–80, Aug. 2018.

[20] A. Narayan and K. Ponnambalam, "Risk-averse stochastic programming approach for microgrid planning under uncertainty," *Renew. Energy*, vol. 101, pp. 399–408, Feb. 2017.

[21] A. Sobu and G. Wu, "Optimal operation planning method for isolated micro grid considering uncertainties of renewable power generations and load demand," in *Proc. IEEE PES Innov. Smart Grid Technol.*, Tianjin, China, May 2012, pp. 1–6.

[22] M. Asensio, G. Muñoz-Delgado, and J. Contreras, "Bi-Level approach to distribution network and renewable energy expansion planning considering demand response," *IEEE Trans. Power Syst.*, vol. 32, no. 6, pp. 4298–4309, Nov. 2017.

[23] B. Liu, X. Huang, and J. Li, "Optimal sizing of distributed generation in a typical island microgrid with time-shifting load," *Proc. Chin. Soc. Elect. Eng.*, vol. 34, no. 25, pp. 4250–4258, 2014.

[24] Z. Wang, Y. Chen, S. Mei, S. Huang, and Y. Xu, "Optimal expansion planning of isolated microgrid with renewable energy resources and controllable loads," *IET Renew. Power Gener.*, vol. 11, no. 7, pp. 931–940, Jul. 2017.

[25] A. Mohsenzadeh, C. Pang, and M.-R. Haghifam, "Determining optimal forming of flexible microgrids in the presence of demand response in smart distribution systems," *IEEE Syst. J.*, vol. 12, no. 4, pp. 3315–3323, Dec. 2018.

[26] J. Feng, B. Zeng, D. Zhao, G. Wu, Z. Liu, and J. Zhang, "Evaluating demand response impacts on capacity credit of renewable distributed generation in smart distribution systems," *IEEE Access*, vol. 6, pp. 14307–14317, 2017.

[27] Z. Liu, F. Wen, and G. Ledwich, "Optimal siting and sizing of distributed generators in distribution systems considering uncertainties," *IEEE Trans. Power Del.*, vol. 26, no. 4, pp. 2541–2551, Oct. 2011.

[28] K. Wang, F. Ciucu, C. Lin, and S. H. Low, "A stochastic power network calculus for integrating renewable energy sources into the power grid," *IEEE J. Sel. Areas Commun.*, vol. 30, no. 6, pp. 1037–1048, Jul. 2012.

[29] W. Hu, P. Wang, and H. B. Gooi, "Toward optimal energy management of microgrids via robust two-stage optimization," *IEEE Trans. Smart Grid*, vol. 9, no. 2, pp. 1161–1174, Mar. 2018.

[30] Y. Ye, Y. Shi, and A. A. O. Tay, "Electro-thermal cycle life model for lithium iron phosphate battery," *J. Power Sources*, vol. 217, pp. 509–518, Nov. 2012.

[31] W. L. F. Degen, "Sharp error bounds for piecewise linear interpolation of planar curves," *Computing*, vol. 79, pp. 143–151, Apr. 2007.

[32] M. H. Amrollahi and S. M. T. Bathaee, "Techno-economic optimization of hybrid photovoltaic/wind generation together with energy storage system in a stand-alone micro-grid subjected to demand response," *Appl. Energy*, vol. 202, pp. 66–77, Sep. 2017.

[33] *NASA Surface Meteorology and Solar Energy-Location*. [Online]. Available: https://eosweb.larc.nasa.gov

[34] *A national assessment of demand response potential*, The Brattle Group, Freeman Sullivan & Co, and Global Energy Partners, Washington, DC, USA, 2009.

GUOLONG MA was born in Luoyang, China, in 1993. He received the bachelor's degree in electrical engineering from the South China University of Technology, Guangzhou, China, in 2017, where he is currently pursuing the master's degree in power system and its automation. His current research interest includes renewable energy integration and distribution system optimization and scheduling.

ZEXIANG CAI was born in Nanjing, China, in 1960. He received the bachelor's degree in electrical engineering from the Huainan Mineral Institute, Hefei, China, in 1982, the master's degree in electrical engineering from the Northeast China Institute of Electrical Power Engineering, in 1985, and the Ph.D. degree in electrical engineering from Tsinghua University, Beijing, China, in 1991. He is currently a Professor with the School of Electric Power Engineering, South China University of Technology, Guangzhou, China. His current research interests include power system stability and control, and power system protective relaying.

PENG XIE was born in Fuzhou, China, in 1989. He received the bachelor's degree from Nanchang University, in 2012, and the master's degree from East China Jiaotong University, in 2015. He is currently pursuing the Ph.D. degree in power system and its automation with the South China University of Technology, Guangzhou, China. His current research interest includes renewable energy integration and distribution system optimization and scheduling.
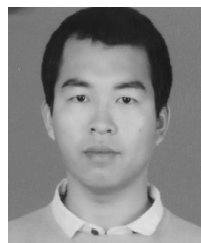
PING LIU was born in Foshan, China, in 1990. He received the B.S. degree in electrical engineering from Beijing Jiaotong University, Beijing, China, in 2013. He is currently pursuing Ph.D. degree with the School of Electric Power, South China University of Technology, Guangzhou, China. His current research interest includes microgrid planning and operation.

SIYANG XIANG was born in Yichang, China, in 1993. He received the bachelor's degree in electrical engineering from the South China University of Technology, Guangzhou, China, in 2016, where he is currently pursuing the master's degree in power system and its automation. His current research interest includes renewable energy integration and distribution system optimization and scheduling.

YUYAN SUN was born in Zhongshan, China, in 1995. She received the bachelor's degree in electrical engineering from the South China University of Technology, Guangzhou, China, in 2018, where she is currently pursuing the master's degree in power system and its automation. Her current research interests include renewable energy integration and distribution system optimization and scheduling.

CAISHAN GUO (S'18) was born in Maoming, China, in 1994. She received the B.E. degree in electrical engineering from the South China University of Technology, Guangzhou, China, in 2016, where she is currently pursuing the Ph.D. degree in power system and its automation. Her current research interests include power system protective relaying, substation automation systems, cloud computing, and computational intelligence.

GUANQUAN DAI was born in Maoming, China, in 1993. He received the bachelor's degree in electrical engineering from the South China University of Technology, Guangzhou, China, in 2017, where he is currently pursuing the master's degree in power system and its automation. His main research interests include power system protection, control, and automation.

● ● ●